

Different associational and conformational behaviors between the second and third repeat fragments in the tau microtubule-binding domain

Katsuhiko Minoura¹, Tian-Ming Yao¹, Koji Tomoo¹, Miho Sumida², Masahiro Sasaki², Taizo Taniguchi^{2,3} and Toshimasa Ishida¹

¹Osaka University of Pharmaceutical Sciences, Takatsuki, Osaka, Japan; ²Behavioral and Medical Sciences Research Consortium, Akashi, Hyogo, Japan; ³Biosignal Research Center, Kobe University, Kobe, Japan

The third repeat fragment (R3) in the four-repeat microtubule-binding domain of the water-soluble tau protein has been considered to play an essential role in the protein's filamentous assembly. To clarify the associational and conformational features that differentiate R3 from the second repeat, R2, the heparin-induced assembly profiles of these peptide fragments were monitored by the thioflavin fluorescence method and electron microscopy. The trifluoroethanol-induced reversible conformational change from a random structure to an α -helical structure, in an aqueous solution, was monitored by CD measurement, and the structure of R2 in trifluoroethanol solution was analyzed by a combination of two-dimensional ¹H-NMR measurements and molecular modeling calculations to facilitate comparison with the structure of R3. The speed of R3 assembly was remarkably faster than that of R2, in spite of their similar

amino acid sequences. The averaged NMR conformers of R2 exhibited the whole-spanning α -helical structure. Similar features observed in R2 and R3 conformers in trifluoroethanol were that the Leu10–Leu20/Lys20 sequence takes a helical structure with the amphipathic-like distribution of the respective side-chains, whereas the C-terminal moieties are both flexible. In contrast, a notable difference was observed at the N-terminal Val1–Lys6 sequence, namely, a helical conformation for R2 and an extended conformation for R3. These conformational behaviors would be associated with the different self-aggregation speeds and seeding reactions between R2 and R3.

Keywords: tau protein; microtubule-binding domain; repeated fragment; self-assembly; amphipathic structure.

Aggregation of the microtubule-associated tau protein is a significant event in neurodegradation [1], because the water-soluble tau protein self-aggregates into a water-insoluble structure known as the paired helical filament (PHF), which is a major component of the pathological lesion in Alzheimer's and other diseases [2]. These aggregates are neurotoxic, as they destroy the cell interior and lead to the development of neuropathological diseases. Therefore, the inhibition of PHF formation may be effective in preventing such a pathological progression.

Although data on the physicochemical behaviors of the tau protein, associated with self-assembly, have increased in recent years, the underlying mechanism at the mole-

cular level remains to be clarified, because the water-soluble tau protein is flexible and takes a random conformation under physiological conditions. It has been reported that the three- or four-repeat microtubule-binding domain (MBD), each repeat consisting of 31 or 32 amino acid residues, located in the C-terminal half (Fig. 1), assumes the core structure of PHF [3] and promotes tau assembly *in vitro* [4]. Therefore, it is important to examine the structural features of the MBD, in order to understand the mechanism underlying PHF formation. In particular, we have focused on clarifying the self-associational and conformational features of the repeat fragments in MBD. Little such data has previously been reported, despite its usefulness in determining the contribution of each repeat fragment to PHF formation.

Recently, we have determined the structure of the third repeat of MBD (R3 in Fig. 1), in water and trifluoroethanol (TFE) solutions, by using the ¹H-NMR method [5,6], and clarified the extended-like structure of the N-terminal VQIVYK sequence and the helical structure of the Leu10–Leu20 sequence, with an amphipathic distribution of the corresponding side-chains, in TFE. This conformational behavior may be associated with the filament formation of MBD, because the VQIVYK local sequence of R3 was reported to play an important role in the assembly of the tau protein into PHF, which is responsible for Alzheimer's lesion [7]. On the other hand, it has been

Correspondence to K. Minoura, Research Center, Osaka University of Pharmaceutical Sciences, 4-20-1 Nasahara, Takatsuki, Osaka 569-1094, Japan. Fax/Tel.: + 81 726 90 1039, E-mail: minoura@gly.oups.ac.jp. or T.-M. Yao, Department of Physical Chemistry, Osaka University of Pharmaceutical Sciences, 4-20-1 Nasahara, Takatsuki, Osaka 569-1094, Japan. Fax/Tel.: + 81 726 90 1068, E-mail: yao@gly.oups.ac.jp
Abbreviations: MBD, microtubule-binding domain; PHF, paired helical filament; TFE, trifluoroethanol; ThS, thioflavin S.
(Received 29 August 2003, revised 12 November 2003, accepted 5 December 2003)

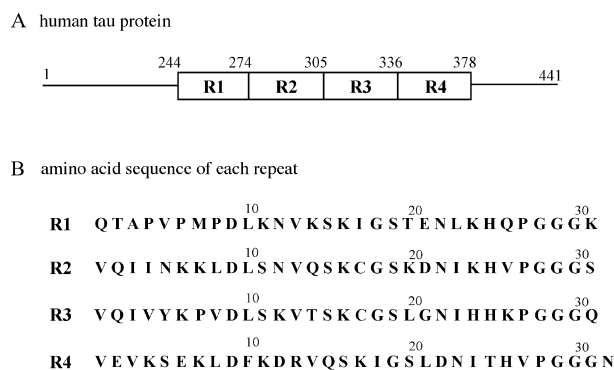


Fig. 1. Schematic representation of the four-repeat microtubule-binding domain (MBD) moiety in the entire human tau protein (A) and the amino acid sequence of each repeat (B). The regions from the first to the fourth repeat fragments in MBD (A) are named R1 to R4, respectively. The numbering of the amino acid residues in (A) refers to the longest isoform of human tau protein (441 residues).

reported that the R2-included and -deleted tau proteins demonstrate a notable difference in their microtubule-binding ability and PHF formation [8–10]; the four-repeat and three-repeat isoforms of the tau MBD are a direct result of the presence or absence of R2, respectively [11]. Therefore, in order to clarify the difference in the associational and conformational behaviors between R3 and R2 repeat fragments, we investigated their assembly profiles by the thioflavin S (ThS) fluorescence method and electron microscopy. Moreover, the TFE-induced conformation of R2 was analyzed by ¹H-NMR spectroscopy and was compared with that of R3. It is important to investigate to what extent their averaged conformations differ in solution (even in a nonphysiological solution), because the reason why R2 does not play as crucial a role as R3 in PHF formation, in spite of their nearly identical N-terminal sequences and the fact that both possess one Cys residue each (Fig. 1) is, as yet, unclarified.

Materials and methods

Peptide

R1, R2, R3 and R4 peptides, corresponding to the first (244–274), second (275–305), third (306–336) and fourth (337–378) repeat fragments of the full-length human tau protein, respectively, were synthesized in the form of lyophilized powders (including trifluoroacetic acid as a counter ion). These peptides were characterized by MS and were purified to > 95.0%, as assessed by reverse-phase HPLC.

Electron microscopy

Each repeat peptide (15 μM) was mixed with 3.8 μM heparin in 50 mM Tris/HCl (pH 7.5). The solution was then incubated at 37 °C for 24 h. For negative-staining electron microscopy, 600-mesh copper grids were used. A drop of peptide solution and a drop of 2% uranyl acetate were placed on the grids. After 2 min, excess fluid was removed from the grids. Negative-staining electron microscopy was

performed using an electron microscope (Hitachi H-600) operated at 75 kV.

Monitoring of aggregation of the MBD repeat fragment by ThS fluorescence

Each repeat peptide was adjusted to a concentration of 15 μM using 50 mM Tris/HCl (pH 7.5) containing 10 μM ThS dye. Aggregation was induced by adding heparin (final concentration 3.8 μM) to the solution, which was then mixed with a pipette prior to measuring the fluorescence. The time-scanning of fluorescence was carried out on a JASCO FP-6500 instrument using a 2-mm quartz cell, in which the temperature was maintained at 37 °C by a circulating water bath. The kinetics of MBD aggregation was analyzed by recording the time-dependent curve of the fluorescence intensity, with excitation at 440 nm and emission at 490 nm. Background fluorescence of the sample was reduced as required.

CD measurement

The sample solution was adjusted to 40 μM in water, TFE, and these mixed solvents, where the pH value was adjusted by adding HCl or NaOH. All measurements at 25 °C were conducted using a JASCO J-820 spectrometer in a cuvette with a 2-mm path length. For each experiment under N₂ gas flow, measurement from 190 to 260 nm was repeated eight times and the results were summed. Then, the molar ellipticity was determined after normalizing the sample concentration. The same experiment was performed at least three times using newly prepared samples; their averaged values are presented below, in the Results and discussion. Data were expressed in terms of a mean residue ellipticity (θ) in units of deg cm²·dmol⁻¹.

NMR measurement

The method used to determine the structure of R2 was the same as that used for R3 [5,6]. The peptide (2 mM) was dissolved in TFE-*d*₂, and its ¹H-NMR spectra were recorded using a Varian unity INOVA500 spectrometer equipped with a variable temperature-control unit. ¹H chemical shifts were referenced to 0 p.p.m. for 3-(trimethylsilyl) propionic acid at 298 K. Owing to the low solubility at pH values of > 5.0, the pH was adjusted to 3.9 by adding HCl or NaOH. In order to trace direct single- and multiple-relayed through-bond connectivities, successively, TOCSY spectra were recorded at mixing times of 40 and 100 ms. The NOESY spectra were also measured at mixing times of 100, 200, and 300 ms. Assuming the same correlation time for all the protons, the offset dependence of the NOESY cross-peaks was used for the estimation of proton–proton distance. The NOE intensities were classified into three groups (strong, medium and weak). The vicinal coupling constants obtained from DQF-COSY measurements were used to estimate the possible torsion angles:

$${}^3J_{\text{HNC}\alpha\text{H}} = 1.9 - 1.4 \cos \theta + 6.4 \cos^2 \theta \quad (1)$$

where $\phi = \theta - 60^\circ$ for the ϕ torsion angle around the C'_{i-1}-N_i-C_α-C'_i bond sequence [12].

Conformational calculations

Three dimensional structures that fulfil the NOE distance and J torsion angle constraints of intramolecular proton pairs were constructed by dynamic simulated annealing calculations [13] using the CNS program [14]. After randomizing the peptide into extended strands, corresponding to each disjointed molecular entity, the initial structures were constructed by referring to the data structures and statistical analysis of the average property. The constructed structure was then annealed for 15 ps at 50 000 K and cooled to 300 K (at a rate of 250 K/step) for 10 ps, and the minimization of more than 5000 steps was continued. The constraints for distances and torsion angles were used as the harmonic potential function. As the input data for distance constraint, the proton-proton pairs were classified into three distance groups according to the NOE intensities: strong (1.8–3.0 Å), medium (1.8–4.0 Å) and weak (1.8–5.0 Å). The torsional constraint was applied to the torsion ϕ angle, i.e. $-120 \pm 40^\circ$ for $^3J_{\text{HNC}\alpha\text{H}} > 8$ Hz, $-75 \pm 25^\circ$ for $^3J_{\text{HNC}\alpha\text{H}} < 6$ Hz, and $-100 \pm 60^\circ$ for the others. The root mean square deviation analyses of energy-minimized structures were carried out using the MOLMOL program [15].

Results and discussion

Different behaviors among four repeat fragments for filament formation

It has been reported that thioflavin dyes, such as ThS, can be used to quantify the filament formation in solution in real time [16]. We used this assay to monitor the filamentous assembly of each repeat MBD peptide, the aggregation of which was induced by adding heparin. The aggregation kinetics was then derived from the time dependence of fluorescence intensity. As shown in Fig. 2A, the fluorescence intensity of R3 reached a maximum within 50 min ($t_{1/2} = \approx 15$ min). However, the presence of dithiothreitol caused a significant decrease in its fluorescence intensity, indicating that the intermolecular disulfide bond formation between the Cys residues of neighboring R3 is a major step for initiating filament formation. In contrast, the increase in ThS intensity was very slow in R2 (Fig. 2B), indicating that the aggregation mechanism of R2 is different from that of R3. As the ThS intensity of R2 also decreased in the presence of dithiothreitol, the filament of R2 may be formed through disulfide bonds. However, R2 showed a considerably different profile from R3, although both peptides contain one Cys residue and possess similar amino acid sequences (Fig. 1B). In order to consider the biological/structural implication of this difference, the effect of seeding for filament formation was investigated. As shown in Fig. 2C,D, a notable difference was observed. The R2 peptide showed an R2-dependent seeding effect, whereas R3 was only

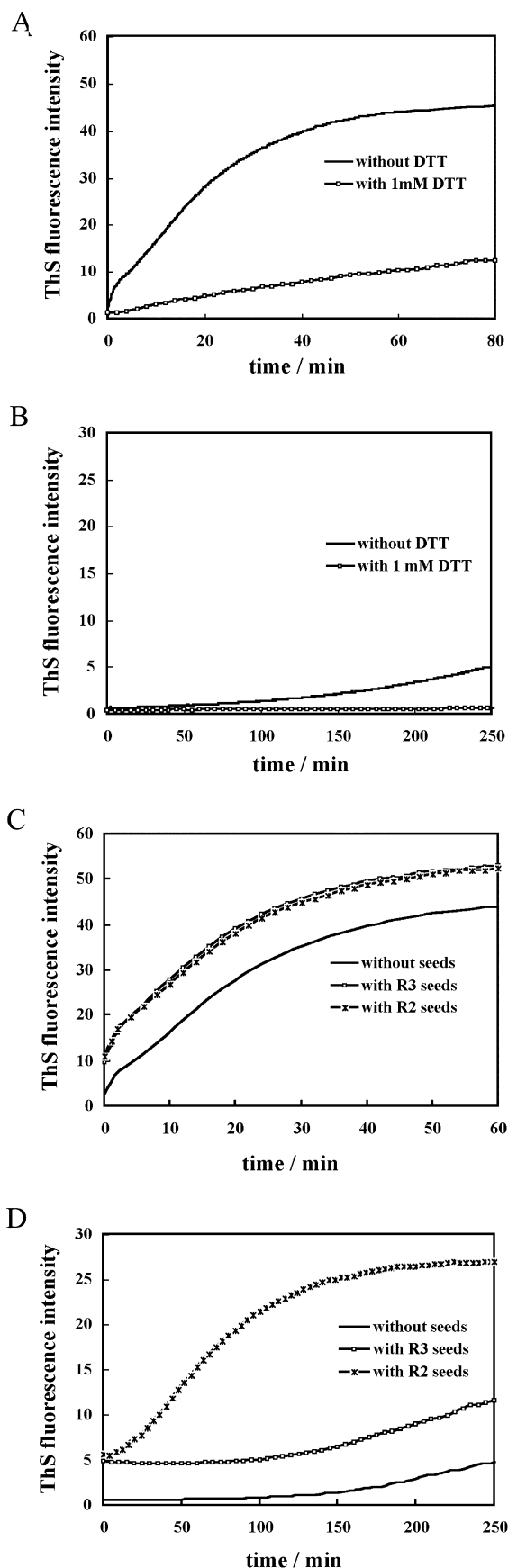


Fig. 2. Heparin-induced *in vitro* aggregation profiles. Heparin-induced *in vitro* aggregation profiles of R3 with and without 1 mM dithiothreitol (A), of R2 with and without 1 mM dithiothreitol (B), and of seeded R3 (C) and R2 (D), as functions of reaction time, monitored based on thioflavin S (ThS) fluorescence intensity.

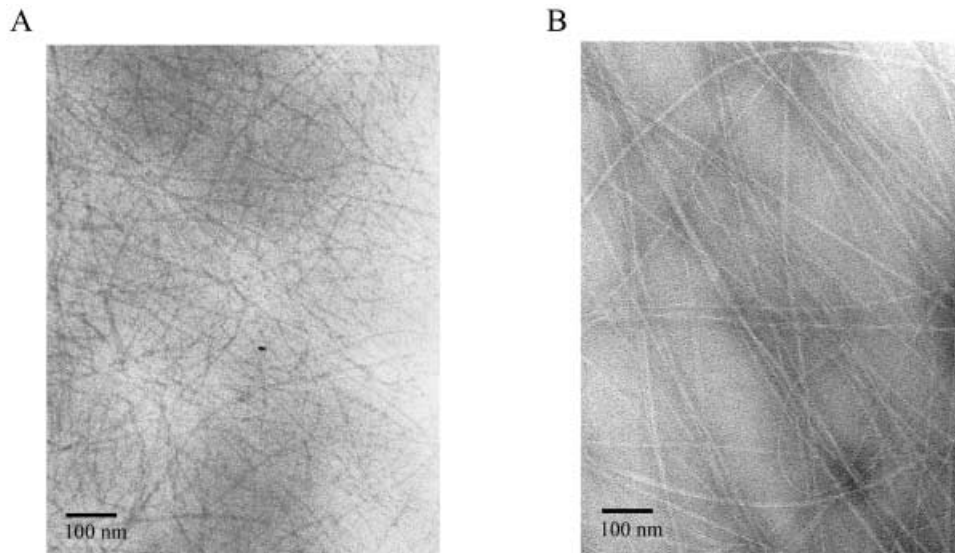


Fig. 3. Electron micrographs of R3 (A) and R2 (B). Samples were negatively stained with 2% uranyl acetate.

slightly affected by any seeding. From these results, it would be reasonable to consider that the R3 peptide aggregates easily, without the help of any template. In contrast, the R2 peptide does not aggregate easily, and its filament formation progresses via a nucleation step, in which the template of homogeneous aggregates is required.

Figure 3 shows the electron micrographs of R2 and R3 filaments. Both R2 and R3 peptides exhibited thin and straight filaments. However, a notable difference was observed in their shapes, that is, the R2 filaments were considerably longer and wider than the R3 filaments.

Compared with R2 fibrils, those of R3 showed a nonphysiological morphology, probably as a result of the high speed of assembly, because the R3 peptide, when mixed with a diluted heparin concentration ($< \approx 1 \mu\text{M}$) formed biologically relevant fibrils similar to those of R2.

The filament formation of MBD was therefore thought to start through the aggregation of R3 and/or R2 peptide, because neither R1 nor R4 peptides showed a lack of ThS fluorescence intensity and filament formation, as judged by EM, under the same experimental conditions.

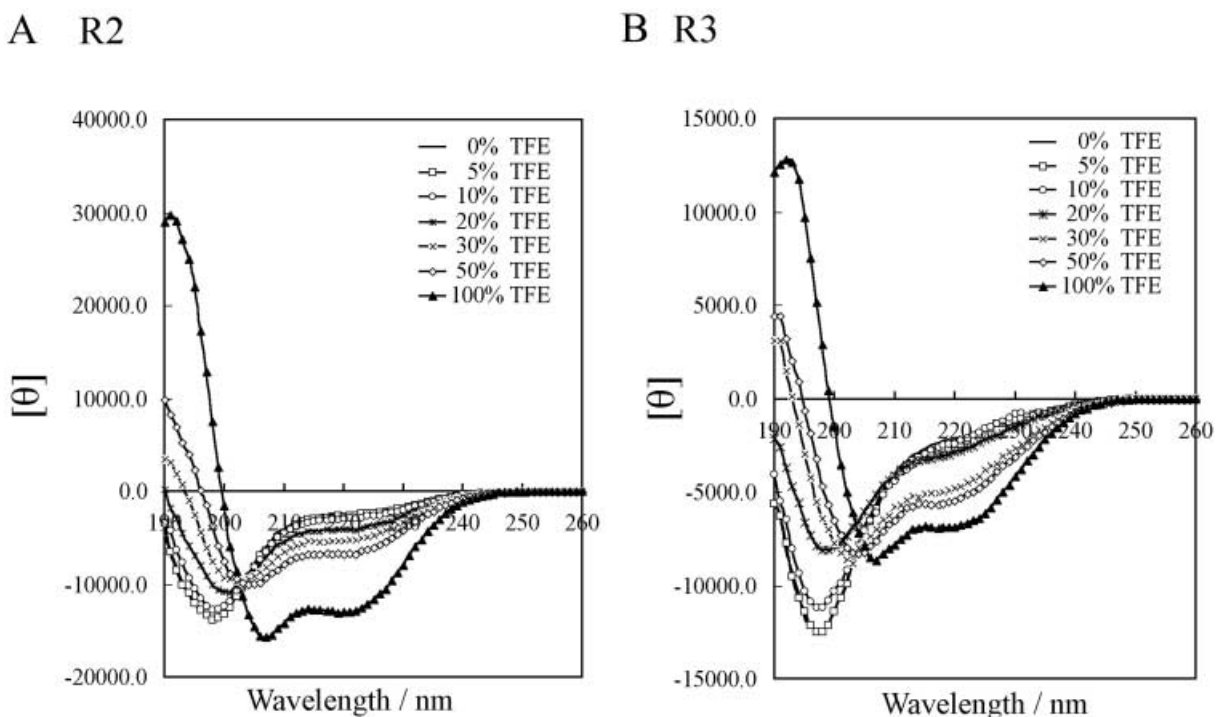


Fig. 4. CD spectra of R2 and R3. CD spectra of R2 (A) and R3 (B) at different ratios of water/trifluoroethanol (TFE) mixture at pH 4.3.

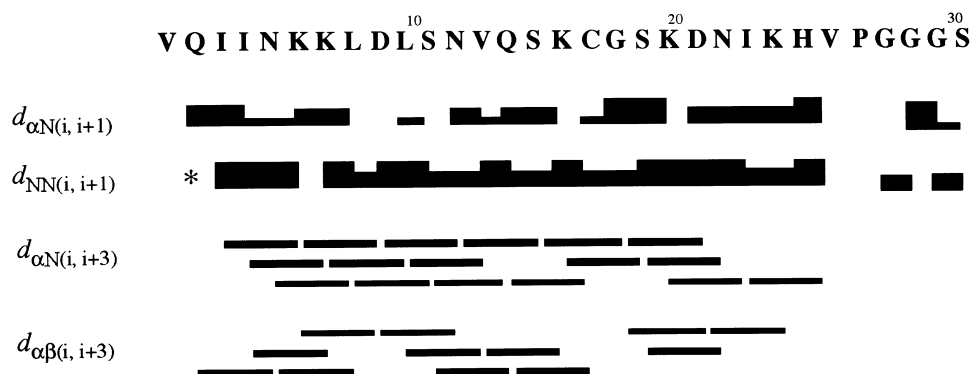


Fig. 5. Diagram of NOE connectivity between neighboring [$d_{\alpha N(i, i+1)}$, $d_{NN(i, i+1)}$, $d_{\alpha N(i, i+3)}$ and $d_{\alpha B(i, i+3)}$] protons. The strength of the observed NOE is represented by the thickness of respective bars.

TFE-induced conformational change

In order to determine, in greater detail, the reason for the above-mentioned difference, it is important to investigate the difference in flexibility and conformational features between R2 and R3 peptides. To estimate their flexibilities, the CD spectra at pH 4.3 were measured at different ratios of the water/TFE mixture (Fig. 4); approximately the same profiles were also observed at pH 7.0. The conformations of R2 and R3 peptides showed a similar solvent-dependent behavior, although their ellipticities were considerably different. Whereas their CD spectra in water predominantly showed a random conformation characterized by a negative peak at ≈ 197 nm, the spectra in TFE indicated an α -helical structure characterized by two negative peaks at ≈ 209 nm and 222 nm. The conformational transitions started at $\approx 20\%$ TFE and the α -helical structure content showed a direct increase in proportion to the TFE concentration. The conformations were reversibly transformed to the random structure upon addition of water to the TFE solution and were scarcely affected by the pH change. No notable time lag was observed between the reversible conformational transitions, indicating that the helical conformations of R2 and R3 peptides are both sufficiently flexible to change their structures, depending on the hydrophobic and hydrophilic balance of the solvent. On the other hand, the calculation from the CD ellipticity [17] indicated a meaningful difference in the α -helical structure content between R2 and R3 peptides, i.e. R2 = 9.7% and R3 = 7.6% at 0% TFE, R2 = 12.2% and R3 = 8% at 10% TFE, R2 = 17.6% and R3 = 12.1% at 20% TFE, R2 = 21.7% and R3 = 17.8% at 30% TFE, R2 = 28.2% and R3 = 20.6% at 50% TFE, and R2 = 53.6% and R3 = 34.2% at 100% TFE. This shows that it is much easier to induce a conformational change of R2 than of R3, and also indicates that the transition energy of R2 is less than that of R3.

Conformation of R2 in TFE solution

The structure of R2 in the TFE solution was analyzed by both $^1\text{H-NMR}$ spectroscopy and molecular modeling calculations; we have previously determined the TFE-induced conformation of R3 by using the same method [5,6]. Proton peak assignments were performed using a combination of (a) connectivity information via scalar

coupling in phase-sensitive TOCSY experiments and (b) sequential NOE networks along the peptide backbone protons. The diagram of short-, medium- and long-range proton–proton connectivity along the peptide backbone, observed by NOESY, is shown in Fig. 5. The orientation around the Val26–Pro27 ω bond was determined to be *trans* from the strong NOE of the $\text{C}\alpha\text{H}$ (Val26)– $\text{C}\delta\text{H}$ (Pro27) proton pair. The NOESY cross-peak pattern among neighboring protons suggested an α -helical structure of the Val1–His25 sequence. Using 374 NOE constraints for proton–proton distances, and 25 $J_{\text{HNC}\alpha\text{H}}$ constraints for ϕ torsion angles, 100 possible conformers were constructed by a dynamic simulated annealing calculation. The statistics of the 20 most stable conformers are summarized in Table 1, and their superposition on the backbone structure is shown in Fig. 6. The constructed conformers exhibited α -helical structures of the Ile3–His25 sequence, whereas the C-terminal Gly–Gly–Gly–Ser sequence was flexible and did

Table 1. Structural statistics of 20 stable structures of the R2 domain.

Structural feature	Value
Number of structures	20
Number of constraints:	
Total number of NOEs	374
Intraresidue NOEs	211
Sequential NOEs	106
Inter-residue NOEs	57
Dihedral angles	25
	Average values (esd)
RMS deviation (N, $\text{C}\alpha$, C') (\AA)	0.68 (25) ^a
RMS deviation from NOE (\AA)	0.069 (2)
NOE violations > 0.10 (\AA)	11.0 (8)
Energy (kcal/mol)	
Overall	315 (6)
NOE	133 (7)
Angle	90 (3)
Bond	25 (1)
Improper	9.0 (8)
van der Waals	58 (4)

^a Calculated from residues 3–20.

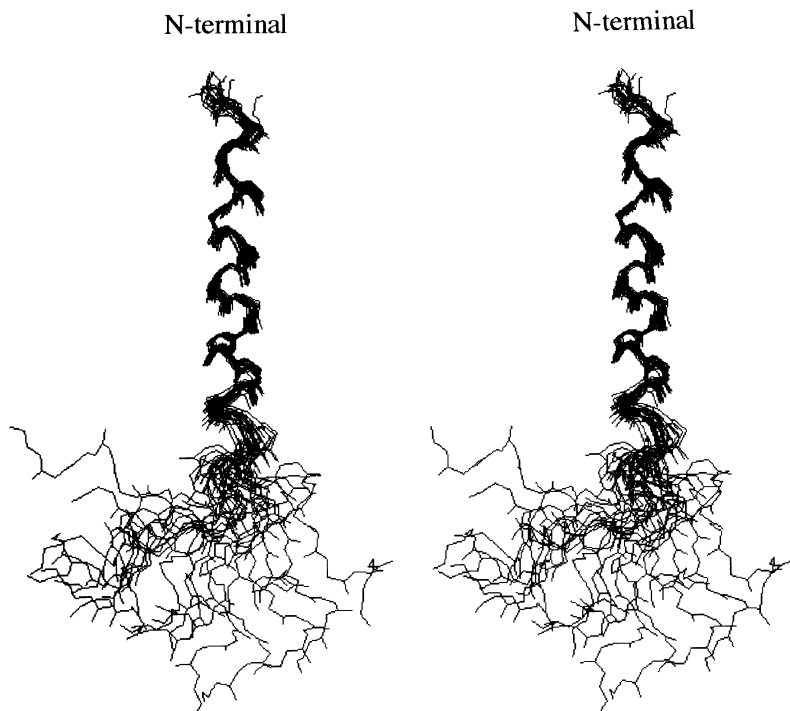


Fig. 6. Stereoscopic superposition of the most stable 20 conformers of R2. Each conformer is projected in order to superimpose on the Ile3–Lys20 sequence. The upper and lower sides of conformers correspond to N- and C-terminal regions, respectively.

not show any definite 3D structure. As the CD spectrum in the TFE solution suggested an $\approx 50\%$ content of the α -helical structure, it can be predicted that the R2 peptide is in equilibrium between equimolar amounts of random and helical conformers; Fig. 6 corresponds to an ensemble of the latter conformers.

Conformational comparison between R2 and R3 in TFE solution

As the NMR data reflect an ensemble of various dynamic conformers, the conformational comparison between R2 and R3 peptides is possible only in terms of the structural features observed commonly in various NMR-constructed conformers of each peptide, and the common features of R2 and R3 backbone conformers are schematically shown in Fig. 7A,B respectively. A similar conformational feature of R2 and R3 peptides can be described as follows. The Leu10–Lys20 sequence of R2 forms an α -helical structure, and the helix wheel drawing of this sequence shows an amphipathic distribution of the respective amino acid residues (Fig. 8A), where the hydrophobic residues, Leu10 and Val13, and the hydrophilic residues, Ser11, Ser15, and Ser19, are arranged on the both sides of the helix axis, respectively, and the polar residues, Asn12, Gln14, Lys16, and Lys20, are located at the interface between both sides. Similar features can also be observed in the conformation of R3 (Fig. 8B).

The remarkable conformational discrepancy between the two peptides can be characterized as follows. The N-terminal Val1–Lys6 sequence of R2 takes a typical α -helical structure, while that of R3 shows an extended-like conformation; this structure has also been observed in aqueous solution [6] and would not be a result of the presence of the Pro7 residue in R3, because this residue

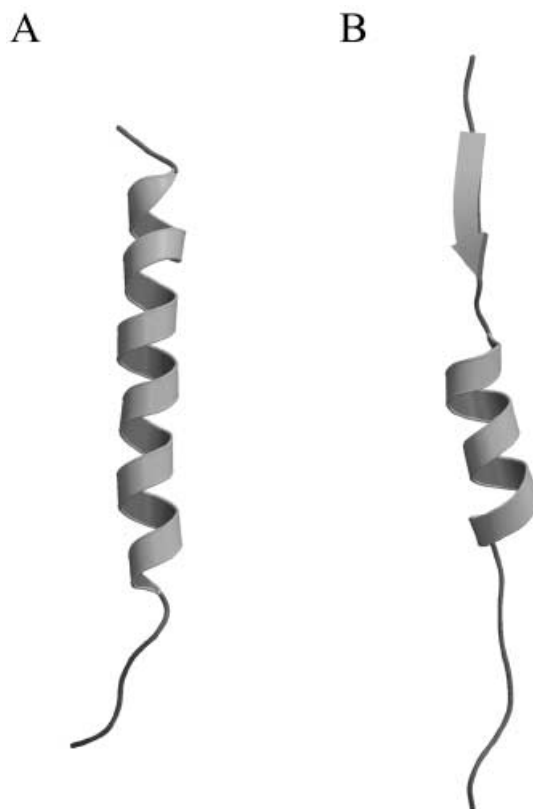


Fig. 7. Average backbone conformations. Comparison of averaged backbone conformations commonly observed in various NMR conformers of R2 (A) and R3 (B). The N- and C-terminal regions correspond to the upper and lower sides, respectively.

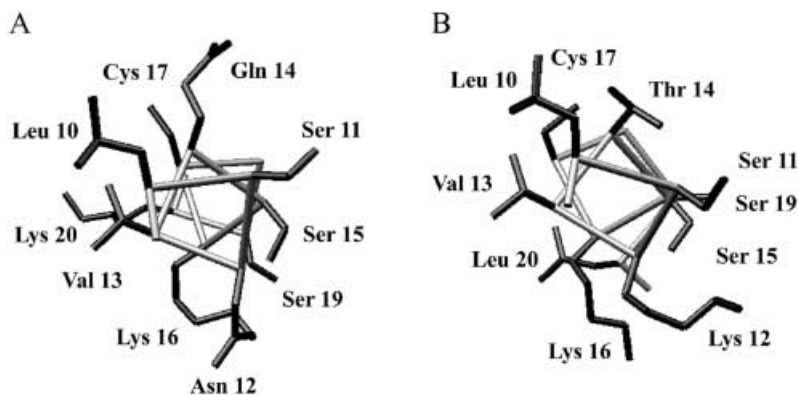


Fig. 8. Helical wheel drawings. Helical wheel drawings of the Leu10–Leu20 sequences of the most stable conformers of R2 (A) and R3 (B), viewed from the N-terminal side.

takes a *trans* orientation with regard to the ω torsion angle both in water and TFE.

This conformational result indicates the following, concerning the difference in time profile between R2 and R3 filament formations (Fig. 2), although the experimental conditions are different. The extended-like structure of the N-terminal VQIVYK sequence in R3 is important for facilitating aggregation without requiring any template for forming an ordered filament structure, whereas the helical structure of the N-terminal VQIINK sequence of R2 is flexible and changes easily into the conformation required in a particular environmental condition, as judged from the very slow aggregation and the rapid template-dependent filament formation.

Concerning the conformation–filament formation relationship of the MBD, the present work proposes the following possibility, namely, an association through the helical structures of R2 and R3 repeats and/or the β -structure-mediated association of the N-terminal VQIVYK sequence in R3. At present, a unified scheme has not yet been established concerning the mechanism of PHF formation, although it has been proposed [18]. The present TFE-induced helical structures of R2 and R3 cannot be directly associated with the PHF aggregation of tau MBD under physiological conditions. However, the speed of three- or four-repeat MBD assembly could be R3-dependent, because a lack of the R3 domain leads to a considerable slow down of the assembly process. Also, the physiological morphology of the MBD filament formation absorbs almost the entire effect of the nonphysiological one of the R3 filament. Therefore, it would be reasonable to consider that the relationship proposed above is likely to occur in the PHF formation of tau protein. This is also suggested from the association through the helical structures with an amphipathic character, which is enthalpy advantageous [6], and the importance of the extended-like VQIVYK sequence as a core structure for the PHF formation of tau protein has been proposed [19].

In conclusion, the present study has clarified, for the first time, the notable difference between the second and third repeat fragments in the tau MBD in terms of (a) self- and seeded-aggregations and (b) the conformation induced by TFE solution. Knowledge of these different conformational behaviors will be helpful in future investigations undertaken to clarify the mechanism underlying the MBD assembly of the tau protein.

Acknowledgements

This work was supported by Grants-in-Aid for Scientific Research from the Ministry of Education, Culture, Sports, Science and Technology of Japan, by JSPS Postdoctoral Fellowship for Foreign Researchers (T.-M. Y), and by The Science Research Promotion Fund of The Promotion and Mutual Aid Corporation for Private Schools of Japan.

References

- Lee, V.M., Goedert, M. & Trojanowski, J.Q. (2001) Neurodegenerative tauopathies. *Annu. Rev. Neurosci.* **24**, 1121–1159.
- Friedhoff, P., Von Bergen, M., Mandelkow, E.-M. & Mandelkow, E. (2000) Structure of tau protein and assembly into paired helical filaments. *Biochim. Biophys. Acta* **1502**, 122–132.
- Priedhoff, F., Von Bergen, M., Mandelkow, E.-M. & Mandelkow, E. (1998) A nucleated assembly mechanism of Alzheimer paired helical filaments. *Proc. Natl Acad. Sci. USA* **95**, 15712–15717.
- Wille, H., Drewes, G., Biernat, J., Mandelkow, E.-M. & Mandelkow, E. (1992) Alzheimer-like paired helical filaments and antiparallel dimers formed from microtubule-associated protein tau *in vitro*. *J. Cell Biol.* **118**, 573–584.
- Minoura, K., Tomoo, K., Ishida, T., Hasegawa, H., Sasaki, M. & Taniguchi, T. (2002) Amphipathic helical behavior of the third repeat fragment in the tau microtubule-binding domain, studied by $^1\text{H-NMR}$ spectroscopy. *Biochem. Biophys. Res. Commun.* **294**, 210–214.
- Minoura, K., Tomoo, K., Ishida, T., Hasegawa, H., Sasaki, M. & Taniguchi, T. (2003) Solvent-dependent conformation of the third repeat fragment in microtubule-binding domain of tau protein, analyzed by $^1\text{H-NMR}$ spectroscopy and molecular modeling calculation. *Bull. Chem. Soc. Jpn* **76**, 1617–1624.
- Von Bergen, M., Friedhoff, P., Biernat, J., Heberle, J., Mandelkow, E.-M. & Mandelkow, E. (2000) Assembly of tau protein into Alzheimer paired helical filaments depends on a local sequence motif (306) VQIVYK (311) forming beta structure. *Proc. Natl Acad. Sci. USA* **97**, 5129–5134.
- Schweers, O., Mandelkow, E.-M., Biernat, J. & Mandelkow, E. (1995) Oxidation of cysteine-322 in the repeat domain of microtubule-associated protein tau controls the *in vivo* assembly of paired helical filament. *Proc. Natl Acad. Sci. USA* **92**, 8463–8467.
- Bhattacharya, K., Rank, K.B., Evans, D.B. & Sharma, S.K. (2001) Role of cysteine-291 and cysteine-322 in the polymerization of human tau into Alzheimer-like filaments. *Biochem. Biophys. Res. Commun.* **285**, 20–26.
- Goode, B.L., Chau, M., Denis, P.E. & Feinstein, S.C. (2000) Structural and functional differences between 3-repeat and 4-repeat tau isoforms. *J. Biol. Chem.* **275**, 38182–38189.

11. Goedert, M. & Spillantini, M.G. (2000) Tau mutations in frontotemporal dementia FTDP-17 and their relevance for Alzheimer's disease. *Biochim. Biophys. Acta* **1502**, 110–121.
12. Bystrov, V.F. (1976) Spin-spin coupling and the conformational states of peptide systems. *Prog. Nucl. Magn. Reson. Spectrosc.* **10**, 41–81.
13. Nilges, M., Clore, G.M. & Gronenborn, A.M. (1988) Determination of three-dimensional structures of proteins from interproton distance data by hybrid distance geometry-dynamical simulated annealing calculations. *FEBS Lett.* **229**, 317–324.
14. Brunger, A.T., Adams, P.D., Clore, G.M., DeLano, W.L., Gros, P., Grosse-Kunstleve, R.W., Jiang, J.S., Kuszewski, J., Nilges, M., Pannu, N.S., Read, R.J., Rice, L.M., Simonson, T. & Warren, G.L. (1998) Crystallography and NMR system: a new software suited for macromolecular structure determination. *Acta Crystallogr.* **D54**, 905–921.
15. Koradi, R., Billeter, M. & Wuthrich, K. (1996) MOLMOL: a program for display and analysis of macromolecular structures. *J. Mol. Graphics* **14**, 51–55.
16. Friedhoff, P., Schneider, A.E.M., Davies, P. & Mandelkow, E. (1998) Rapid assembly of Alzheimer-like paired helical filaments from microtubule-associated protein tau monitored by fluorescence in solution. *Biochemistry* **37**, 10223–10230.
17. Chen, Y.H., Yang, J.T. & Martinez, H.M. (1972) Determination of the secondary structures of proteins by circular dichroism and optical rotatory dispersion. *Biochemistry* **11**, 4120–4131.
18. Barghorn, S. & Mandelkow, E. (2002) Toward a unified scheme for the aggregation of tau into Alzheimer paired helical filaments. *Biochemistry* **41**, 14885–14896.
19. Von Bergen, M., Barghorn, S., Li, L., Marx, A., Biernat, J., Mandelkow, E.-M. & Mandelkow, E. (2001) Mutations of tau protein in frontotemporal dementia promote aggregation of paired helical filaments by enhancing local β -structure. *J. Biol. Chem.* **276**, 48165–48174.